Int. J. Heat Mass Transfer. Vol. 35, No. 5, pp. 1197–1207, 1992
Printed in Great Britain

0017–9310/92 $5.00 + 0.00

Analysis and experiment of non-Darcian convection in horizontal square packed-sphere channels—II. Mixed convection

F. C. CHOU, C. J. CHENG and W. Y. LIEN†

Department of Mechanical Engineering, National Central University, Chung-li 32054, Taiwan, Republic of China

(*Received* 5 *November* 1990 *and in final form* 2 *May* 1991)

Abstract—This paper presents an analysis and experiment of fully developed non-Darcian mixed convection in horizontal packed-sphere channels. The non-Darcian effects of no-slip boundary, flow inertia, channeling and thermal dispersion are considered. The theoretical results are found to be in agreement with the experimental results for the channel of $D_c/d = 10$, but the predictions of Nusselt number are higher than the experimental data, partly due to theoretical overestimation of the thermal dispersion effect and partly due to the entrance effect existing in the experiments for $D_c/d = 19$. The analysis shows that the buoyancy effect significantly affects the secondary flow structure and heat transfer rate when the Peclet number is low, but even under a fixed Rayleigh number, the effect of buoyancy will be suppressed when the Peclet number increases. The values of Nusselt number in the fully developed region depend on Rayleigh number, Peclet number and the diameter ratio of channel to sphere (D_c/d).

1. INTRODUCTION

THE RESEARCH of heat transfer in porous media has been the subject of many recent studies due to the increasing need for better understanding of the associated transport process in various engineering systems. The great majority of previous studies on the convective heat transfer in porous media were confined to natural convection or forced convection; the study of mixed convection is still limited.

Wooding [1], Prats [2], Sutton [3], and Homsy and Sherwood [4] made early theoretical investigations of combined free and forced convection in a porous layer. However, the main emphasis of these papers was on the instability of the flow field and the determination of the condition which would lead to mixed convection. With reference to the experiments, very few studies were reported. Combarnous and Bia's work [5] was one of the first studies to use experiment and numerical computation on the effect of mean flow on the onset of convection in a porous medium bounded by isothermal planes. By using the similarity and integral methods, Cheng [6, 7] conducted a series of studies on mixed convection over vertical, inclined and horizontal plates in porous media. Minkowycz *et al.* [8] extended Cheng's work by employing local non-similarity methods to obtain a solution for mixed convection over a horizontal plate in a porous medium. Haajizadeh and Tien [9] investigated the mixed convective flow through a horizontal porous channel connecting two reservoirs. Joshi and Gebhart [10] studied the mixed convection in a porous medium adjacent to a vertical uniform heat flux surface. Oosthuizen [11] reported the mixed convection over a heated horizontal plate in a porous medium mounted below an impervious adiabatic horizontal surface. Prasad *et al.* [12] studied the mixed convection in a two-dimensional horizontal porous layer with localized heating from below. It is noted that all the above-mentioned theoretical studies adopted Darcy's law to formulate the problems.

Recently, Chandrasekhara and Namboodiri [13] used a non-Darcian model which included the variations of permeability and thermal conductivity to study the mixed convection over inclined surfaces, and found that these variations affect the heat transfer significantly. Lai and Kulacki [14] used the similarity method and a non-Darcian model which includes the inertia effect to study the mixed convection over horizontal plates in a porous medium. There were also some studies on non-Darcian forced convection over flat plates in porous media or in cylindrical packed beds reported by Beckerman and Viskanta [15], Cheng and Zhu [16], Renken and Poulikakos [17] and Hunt and Tien [18]. To the best of the authors' knowledge, a theoretical and experimental study of non-Darcian mixed convection, in which the effects of inertia, boundary, channeling and thermal dispersion are included, has not been reported. The aim of the present paper is to study numerically and experimentally the non-Darcian mixed convection in the fully developed region of horizontal square channels filled with packed spheres. The results shown are quite different from the mixed convection in a channel without packed spheres, such as high secondary flow intensity near the vertical side walls and suppression of the

† Present address: Power Mechanical Engineering Department, Tsing-Hua University, Hsin-chu, Taiwan, Republic of China.

NOMENCLATURE

A	cross-sectional area
a	width of rectangular channel
a_1, a_2	coefficients used in porosity variation
a_3	thermal dispersion damping constant
b	height of rectangular channel
C	inertial coefficient, $1.75(1-\varepsilon)/(d\varepsilon^3)$
c_p	specific heat at constant pressure
d	sphere diameter
Da	Darcian number, K_x/d^2
D_e	equivalent hydraulic diameter, $4A/S$
g	acceleration due to gravity
h	heat transfer coefficient
K	permeability, $d^2\varepsilon^3/(150(1-\varepsilon)^2)$
k	thermal conductivity
l	mixing length
M, N	number of divisions in the X and Y directions
Nu	Nusselt number, $\bar{h}D_e/k_f$
n	inward normal
p	pressure
Pe	Peclet number, $Pr\,Re$
Pr	Prandtl number, ν_f/α_f
q_w	prescribed uniform heat flux
Ra	Rayleigh number, $g\beta q_w d^4/(\nu_f\alpha_f k_f)$
Ra_{cr}	critical Rayleigh number for the onset of buoyancy effect
Re	Reynolds number based on the sphere diameter, $\langle\bar{w}\rangle d/\nu_f$
S	circumference of cross-section
T	temperature
t	thickness of channel wall
U, V, W	dimensionless velocities in the X, Y, Z directions
u, v, w	velocity components in the x, y, z directions
X, Y, Z	dimensionless rectangular coordinates
x, y, z	rectangular coordinates.

Greek symbols

α	thermal diffusivity
β	coefficient of thermal expansion
γ	coefficient in dispersion conductivity
ε	porosity
θ	dimensionless temperature
μ	dynamic viscosity
ν	kinematic viscosity
ξ	vorticity
ρ	density
ψ	stream function.

Subscripts

c	characteristic quantity
cr	critical value
d	dispersion
e	effective
f	fluid
i	inlet
o	stagnant
w	wall
∞	quantity in the core region.

buoyancy effect by the thermal dispersion effect, and thus the values of Nusselt number in the fully developed region depend on the Rayleigh number, Peclet number and the diameter ratio of channel to sphere (D_e/d).

2. EXPERIMENTAL APPARATUS AND PROCEDURES

The experimental apparatus is shown in Fig. 1. The heated test section is preceded by a constant head tank with an overflow bypass for water head control and a 10 cm long channel for flow development before entering the test section, since the hydraulic entrance region is important only for distance of order $O(Kw/\nu_f)$ [19], where K is the permeability of the porous medium, w is the axial fluid velocity, and ν_f is the kinematic viscosity of the fluid. The heated section was made of a 4.75×4.75 cm stainless steel square channel of length 65 cm and a 9.5×9.5 cm aluminum square channel of length 40 cm with 2 mm wall thickness. The square channels are packed with 5 mm diameter glass spheres. The experiments in the two channels are described as cases 1 and 2 in Table 1. Special care was taken in packing the beads to ensure uniformity in the structure of the porous medium. The spheres were poured randomly into the channel, levelled and then shook. This procedure was repeated until no more beads could be placed into the channel. Two stainless steel screens were placed at the inlet and outlet of the channel to hold the beads in place. The measured global porosity for the whole packed-sphere channel is 0.365 for the stainless steel channel and 0.35 for the aluminum channel. Electric power from four auto-transformers provided Joulean heating for four main heaters on four channel walls. Guard heaters were placed outside of the main heaters to prevent heat loss from the main heaters to the surroundings. The inlet fluid bulk temperature was measured in the fluid at the center of the inlet of the channel. The volumetric flow rate was measured by using a measuring glass and a stop watch.

The value of heat flux to the fluid was required in the calculation of the heat transfer coefficient. The power for each heater was measured with a digital multimeter and a standard shunt resistor. Each main heater was adjusted to give equal power. The value of heat flux was determined by the total power dis-

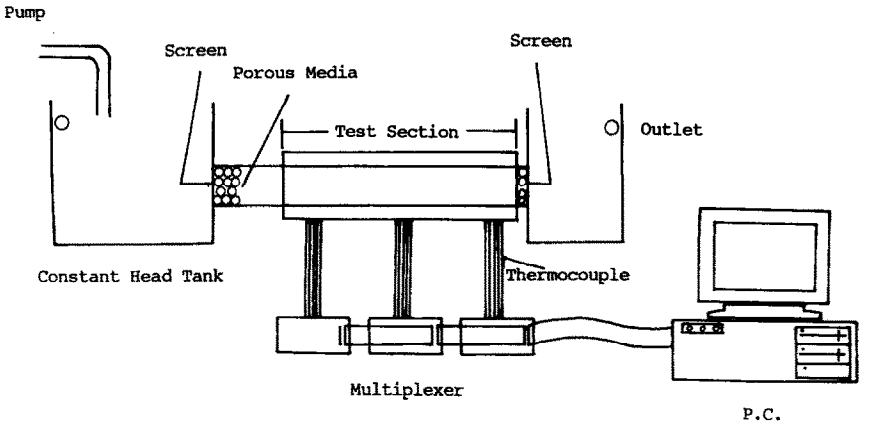

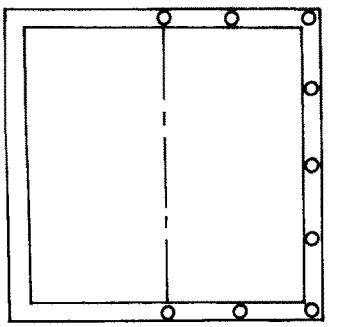

FIG. 1. (a) Experimental apparatus. (b) Schematic of thermocouple set-up.

sipation and the heated area. The variation of wall temperature was measured by nine copper–constantan T-type thermocouples at a cross-section. These nine thermocouples were arranged circumferentially as shown in Fig. 1(b). The average wall temperature was calculated by averaging the readings of the nine copper–constantan thermocouples which were placed at an axial position located 50 cm and 35 cm from the entrance of the heated section in cases 1 and 2, respectively. Prior to installation the thermocouples were calibrated using an ice bath. The overall accuracy are found to be well within $\pm 0.1^{\circ}C$.

Water was chosen as the working fluid because of its availability and wide application. The test generally proceeded by maintaining flow rate, input power and inlet fluid temperature fixed. After a steady state was

Table 1. Brief description of the experiments

The case of experiment	Case 1	Case 2
Dimension of channel	$4.75 \times 4.75 \times 85$ cm	$9.5 \times 9.5 \times 60$ cm
Material of channel	stainless steel	aluminum
Length for hydraulic development	10 cm	10 cm
Length of heated section	65 cm	40 cm
Location from the entrance for thermocouples	50 cm	35 cm
Average porosity $\bar{\varepsilon}$	0.365	0.35

reached, the variation of wall temperatures was recorded. It is sufficient to determine the average wall temperature with the nine temperature readings for the half circumference under the condition of symmetry. The flow rate, inlet fluid bulk temperature, and electric power input were also recorded. The local bulk mean temperature of the fluid at the measuring section was calculated by the values of inlet temperature, flow rate and power input. The fluid enthalpy rise could be a double check to the electric power inputs by measuring the bulk fluid temperature in the mixing chamber. The experimental errors in heat balance were found to be less than 4%. The average wall temperature was calculated by using Simpson's rule for the measured data of nine thermocouples at a cross-section. The nine thermocouples connect through a multiplexer to a personal computer. The local heat transfer coefficient h was calculated by the local heat flux, average wall temperature and the local bulk mean fluid temperature. The evaluation of Nusselt number is based on the equivalent hydraulic diameter D_e and the fluid conductivity k_f as follows:

$$Nu = \bar{h}D_e/k_f = q_w D_e/[k_f(\bar{T}_w - T_b)] \quad (1)$$

where q_w is the heat flux imposed at the outer surface of channel walls, and $\bar{T}_w$ and T_b are the averaged wall temperature and bulk mean fluid temperature. All of the fluid properties (density, specific heat, dynamic viscosity and thermal conductivity) were evaluated at the local film temperature which is the arithmetic mean of local bulk fluid temperature and average wall temperature.

The procedure to collect experimental data was repeated rigorously for each test run. A steady state condition was said to be reached when the deviations of wall temperatures and local bulk fluid temperature were all within ± 0.1°C for 30 min. After each test run the channel was emptied, flushed and refilled with water. The experimental uncertainties in Nusselt number, mainly due to experimental errors in heat balance and temperature measurements, were estimated to be in the range of 11–16%. The largest uncertainties occurred when the temperature difference $(\bar{T}_w - T_b)$ was smaller.

3. THEORETICAL ANALYSIS

The present analysis uses the volume-averaged equations which include non-Darcian effects such as no-slip boundary, flow inertia, channeling and thermal dispersion as used in Hunt and Tien [18]. In vectorial notation, the steady three-dimensional generalizations of continuity, momentum and energy equations in a porous medium are

$$\nabla \cdot \langle v \rangle = 0 \quad (2)$$

$$(\rho/\varepsilon^2)\langle v \cdot \nabla V \rangle = -\nabla \langle p \rangle + \rho g - (\mu/K)\langle v \rangle - \rho C |\langle v \rangle| \langle v \rangle + (\mu/\varepsilon)\nabla^2 \langle v \rangle \quad (3)$$

$$\rho c_p \langle v \rangle \cdot \nabla \langle T \rangle = \nabla(k_e \nabla \langle T \rangle) \quad (4)$$

where $\langle\ \rangle$ represents a volume-averaged quantity, v, p and T are the local velocity, pressure and temperature, ρ and μ are the fluid density and viscosity, ε is the porosity, K and C are the permeability and inertial coefficient, and k_e is the effective conductivity.

The physical configuration and the coordinate system are shown in Fig. 2 for the present problem. Consider a steady laminar flow in both the hydrodynamically and thermally fully developed region of a horizontal square packed-sphere channel heated with axially uniform heat input and peripherally uniform wall temperature. The Boussinesq approximation is used to characterize the effect of free convection. Viscous dissipation and the compressibility effect in the energy equation are neglected. With the following variables

$$X = x/d, \quad Y = y/d, \quad U = \langle u \rangle/(\alpha_f/d),$$
$$V = \langle v \rangle/(\alpha_f/d), \quad W = \langle w \rangle/\langle \bar{w} \rangle,$$
$$\theta = (T_w - \langle T \rangle)/\theta_c, \quad \theta_c = q_w d/k_f,$$
$$Da = K_x/d^2, \quad Re = \langle \bar{w} \rangle d/\nu, \quad Pr = \nu_f/\alpha_f,$$
$$Pe = Pr\,Re, \quad Ra = g\beta q_w d^4/(\nu_f \alpha_f k_f) \quad (5)$$

and introducing the stream function and vorticity

$$U = \partial\psi/\partial Y, \quad V = -\partial\psi/\partial X \quad (6)$$

$$\xi = \partial U/\partial Y - \partial V/\partial X = \nabla^2\psi \quad (7)$$

the governing equations can be obtained

$$\nabla^2\psi = \xi \quad (8)$$

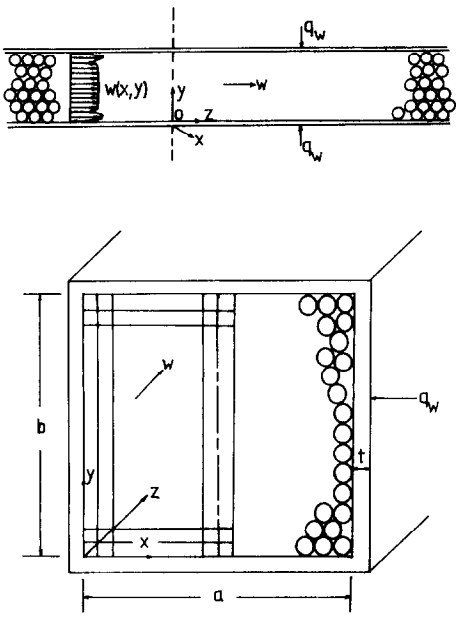

FIG. 2. Schematic for the numerical solution and the coordinate system.

$$(U\partial\xi/\partial X+V\partial\xi/\partial Y)/(\varepsilon Pr)$$
$$+\{U[(\partial V/\partial X)(\partial\varepsilon/\partial X)$$
$$-(\partial U/\partial X)(\partial\varepsilon/\partial Y)]$$
$$+V[(\partial V/\partial Y)(\partial\varepsilon/\partial X)$$
$$-(\partial U/\partial Y)(\partial\varepsilon/\partial Y)]\}/(\varepsilon^2 Pr) = -(\varepsilon d^2/K)\xi$$
$$+\nabla^2\xi+300(1-\varepsilon)(U\partial\varepsilon/\partial Y-V\partial\varepsilon/\partial X)/\varepsilon^3$$
$$-2\varepsilon Cd(U\partial U/\partial Y-V\partial V/\partial X)/Pr$$
$$+1.75(2-\varepsilon)(U^2\partial\varepsilon/\partial Y-V^2\partial\varepsilon/\partial X)/(\varepsilon^3 Pr)$$
$$+\varepsilon Ra(\partial\theta/\partial X)+Ra\,\theta(\partial\varepsilon/\partial X) \quad (9)$$

$$(U\partial W/\partial X+V\partial W/\partial Y)/(\varepsilon Pr)$$
$$=\varepsilon[-K_\infty(\mathrm{d}p/\mathrm{d}z)/(\mu\langle\bar{w}\rangle)]/Da-(\varepsilon d^2/K)W$$
$$-\varepsilon Cd\,ReW^2+\nabla^2 W \quad (10)$$

$$U\partial\theta/\partial X+V\partial\theta/\partial Y$$
$$-4Wd/D_e=(\partial/\partial X)[(k_e/k_f)(\partial\theta/\partial X)]$$
$$+(\partial/\partial Y)[(k_e/k_f)(\partial\theta/\partial Y)] \quad (11)$$

where $\nabla^2=(\partial^2/\partial X^2+\partial^2/\partial Y^2)$, the subscripts ∞ and f represent the values in the core region and the fluid state, respectively, and D_e is the equivalent hydraulic diameter. The Darcian number, Da, relates the permeability to the particle size. The vorticity transport equation (9) is obtained by cross-differentiation of equation (3) to eliminate the pressure term. It is noteworthy that the axial convective term in energy equation (11) for the fully developed region had been transformed to $4Wd/D_e$ by applying the conservation of energy:

$$\partial\langle T\rangle/\partial z=\mathrm{d}\langle T_b\rangle/\mathrm{d}z=\mathrm{d}T_w/\mathrm{d}z=4q_w/(\rho c_p\langle\bar{w}\rangle D_e). \quad (12)$$

From the experimental results of Benenati and Brosilow [20], the porosity, ε, can be represented approximately by a decaying-cosine function as mentioned by Hunt and Tien [18]:

$$\varepsilon=\varepsilon_\infty[1+a_1\exp(-a_2 n/d)\cdot\cos(2\pi n/d)] \quad (13)$$

where ε_∞ is the porosity at the core region, n is the distance from the wall in the inward normal direction, d is the particle diameter, and a_1 and a_2 are empirical coefficients which depend on the packing condition and particle size. The coefficients $a_1=0.43$ and $a_2=3$ are used in the present work, as used by Renken and Poulikakos [17], because the rectangular channel with aspect ratio 2 used in ref. [17] is quite similar to the square channel used in the present work. The values of ε_∞ are determined to be 0.363 and 0.348 to meet the measured global porosity in cases 1 and 2, respectively. For a liquid-saturated porous medium the permeability, K, and the flow inertial parameter, C, depend on the matrix porosity and sphere diameter which are given by the relations developed by Ergun [21]:

$$K=d^2\varepsilon^3/(150(1-\varepsilon)^2) \quad (14)$$

$$C=1.75(1-\varepsilon)/(d\varepsilon^3). \quad (15)$$

The effective conductivity, k_e, is composed of the sum of the stagnant and dispersion conductivities, $k_e=k_o+k_d$. The value of stagnant conductivity depends on the porosity variation and the conductivities of the fluid and solid. Since the thermal conductivity of glass is very close to that of water, $k_o/k_f=1$ is used in the present work. It has been shown in Renken and Poulikakos [17] that neglecting the effect of stagnant conductivity for water and glass spheres works well. The dispersion conductivity, k_d, incorporates the additional thermal transport due to the fluid's tortuous path around the solid particles. This quantity is proportional to the product of the local velocity, a constant γ_∞, and wall function:

$$k_d=\gamma_\infty\rho c_p|\langle v\rangle|l(n)$$
$$=k_f\gamma_\infty Pe[\sqrt{((U^2+V^2)/Pe^2+W^2)}]l(n)/d \quad (16)$$

where $l(n)$ is the wall function for thermal dispersion damping near the wall which is given by Kuo and Tien [22]:

$$l(n)=d\{1-\exp[-n/(\delta d)]\} \quad (17)$$

where δ is an empirical constant. There are two different sources to show the wall effect on thermal dispersion. First, the no-slip boundary condition and the near wall porosity variation modify the velocity distribution near the wall. Second, the mixing of the local fluid stream would be reduced by the presence of a wall. The value $\gamma_\infty=0.07$ was found by Kuo and Tien [22] from the mixing-length concept and statistical averaging process. The empirical constant $\delta=1$ was obtained by the comparison of theoretical and experimental results for the forced convection in Part I of this work [23].

Equations (8)–(16) contain four parameters Pr, Ra, Re and Pe. For a fixed fluid flowing through a channel of fixed aspect ratio, Reynolds number Re, Rayleigh number Ra, and Peclet number Pe govern the flow and heat transfer characteristics. The Prandtl number Pr is assigned 6.5 for water throughout this work. Because of symmetry, it suffices to solve the problem in a half region of the square channel such as that shown in Fig. 2. The boundary conditions are

$$U=V=W=\theta=0 \quad \text{at the channel wall}$$
$$U=\partial V/\partial X=\partial W/\partial X=\partial\theta/\partial X=0$$
$$\text{at the symmetric plane } x=a/2. \quad (18)$$

4. NUMERICAL METHOD OF SOLUTION

To obtain the numerical solutions from the governing equations (8)–(11), a finite-difference scheme is used. Since these equations are coupled with each other, they should be solved simultaneously. The procedures for solving equations (8)–(11) and the related boundary conditions of equation (18) are as follows.

(1) The variations of porosity ε, permeability K and flow inertial coefficient C for the whole calculation domain are obtained from equations (13) to (15).

(2) Assign boundary values and guessed initial values of U, V, W, ψ, ξ and θ.

(3) The stream function ψ at each node can be obtained by solving equation (8) from the values of ξ at each node.

(4) The velocity components U and V can be computed from equation (6).

(5) The values of ξ at the boundary can be calculated from equation (7) and the associated boundary conditions for ψ.

(6) Using the values of U and V from step 4, the boundary vorticity from step 5 and the distribution of θ from step 9, the interior vorticity ξ can be solved by equation (8).

(7) Using the same values of U and V, equation (14) can be solved for W. Check whether the average dimensionless axial velocity $W = \langle \bar{w} \rangle / \langle \bar{w} \rangle$ is equal to 1.0. Otherwise, adjust the value of the pressure term $-K_x(\mathrm{d}p/\mathrm{d}z)/(\mu\langle \bar{w} \rangle)$ in equation (10) to meet the requirement.

(8) Using the values of U, V and W from steps 4 and 7, the variation of dispersion conductivity can be calculated by equation (16).

(9) The interior θ can then be obtained by equation (11).

(10) Steps 3–9 are repeated until the following criterion is satisfied:

$$\text{Error} = \sum_{ij} |(\theta^{n+1} - \theta^n)/\theta^n| / (M \times N) < 10^{-5} \quad (19)$$

where M and N are the number of divisions in the X and Y directions, respectively.

After the temperature field is obtained, the computation of the Nusselt number is of practical interest. The Nusselt number is evaluated on the basis of the overall energy balance:

$$Nu = \bar{h} D_e / k_f = (D_e/d)(1/\theta_b) \quad (20)$$

where b denotes the bulk quantity.

5. RESULTS AND DISCUSSION

To track accurately the near-wall porosity variation and the near-wall damping of dispersion conductivity, a non-uniform grid system ($\Delta X_i = 1.05 \Delta X_{i-1}$, $\Delta Y_j = 1.05 \Delta Y_{j-1}$) is used. The numerical results should be independent of the number of non-uniform grids used. Therefore, a numerical experiment was made and the results are shown in Table 2 with $Pr = 6.5$ for the cases of $Pe = 10$ and 100 with $D_e/d = 10$, and $Pe = 30$ and 100 with $D_e/d = 19$. It is seen that the deviations of computed Nu with $M \times N = 30 \times 60$, 40×80 and 60×120 are all less than 1% for $D_e/d = 10$. Thus $M \times N = 30 \times 60$ was used throughout the work for the cases of $D_e/d = 10$. The deviations of Nu with $M \times N = 38 \times 76$ and 60×120 are all less than 1% for both $Pe = 30$ and 100 and $D_e/d = 19$, thus $M \times N = 38 \times 76$ was used throughout the work for $D_e/d = 19$.

Table 2. Numerical experiments on the non-uniform grid system for the cases of $D_e/d = 10$ and 19 and $Ra = 10^5$

Pe	$M \times N$	Nu
(a) $D_e/d = 10$		
10	30×60	22.113
	40×80	22.046
	60×120	22.001
100	30×60	22.897
	40×80	22.921
	60×120	22.973
(b) $D_e/d = 19$		
30	38×76	31.712
	60×120	31.423
100	38×76	33.989
	60×120	34.304

To illustrate the effect of buoyancy on flow and heat transfer characteristics, the isotherm and streamline patterns are shown in Fig. 3 for the cases of $Ra = 10^5$, $Pe = 10$, 40 and 100, and $D_e/d = 10$, and the cases of $Ra = 10^5$, $Pe = 30$, 40 and 100, and $D_e/d = 19$ are shown in Fig. 4. From equation (6), the magnitude of the local velocity of secondary flow is inversely proportional to the distance between two nearby streamlines. The main pair of eddies is driven by the non-zero temperature gradient in the horizontal direction near the vertical heated wall. It is seen that there exists a higher secondary flow speed in the region near the vertical wall than that in the central region. This is caused by the channeling effect which is due to the higher porosity in the near-wall region. It is also seen that even under the same set of Ra and Pe, both the near-wall secondary flow velocity and the strength of secondary flow are higher in the cases of $D_e/d = 19$ than those in the cases of $D_e/d = 10$, and consequently a higher heat transfer rate will be induced in the cases of $D_e/d = 19$. The above phenomenon is caused by the stronger buoyancy effect in the cases of $D_e/d = 19$ rather than $D_e/d = 10$, because the magnitude of the buoyancy effect is affected not only by heat flux, q_w, as shown in the definition of Rayleigh number, but also the length of heated wall which is shown in the form of D_e/d.

In the central region of the square channel, an adverse temperature gradient in the vertical direction appears near the bottom of the heated horizontal wall due to the thermal boundary condition. As shown in Figs. 3(a) and 4(a) for the cases of $Pe = 10$ with $D_e/d = 10$ and $Pe = 30$ with $D_e/d = 19$, respectively, the adverse temperature gradient induces a second pair of counter-rotating eddies, and isotherms are distorted due to the motion of the second eddy which brings the heated fluid flowing upward along the central symmetric line. The effect of thermal dispersion is relatively weak for low flow rates ($Pe = 10$ or 30),

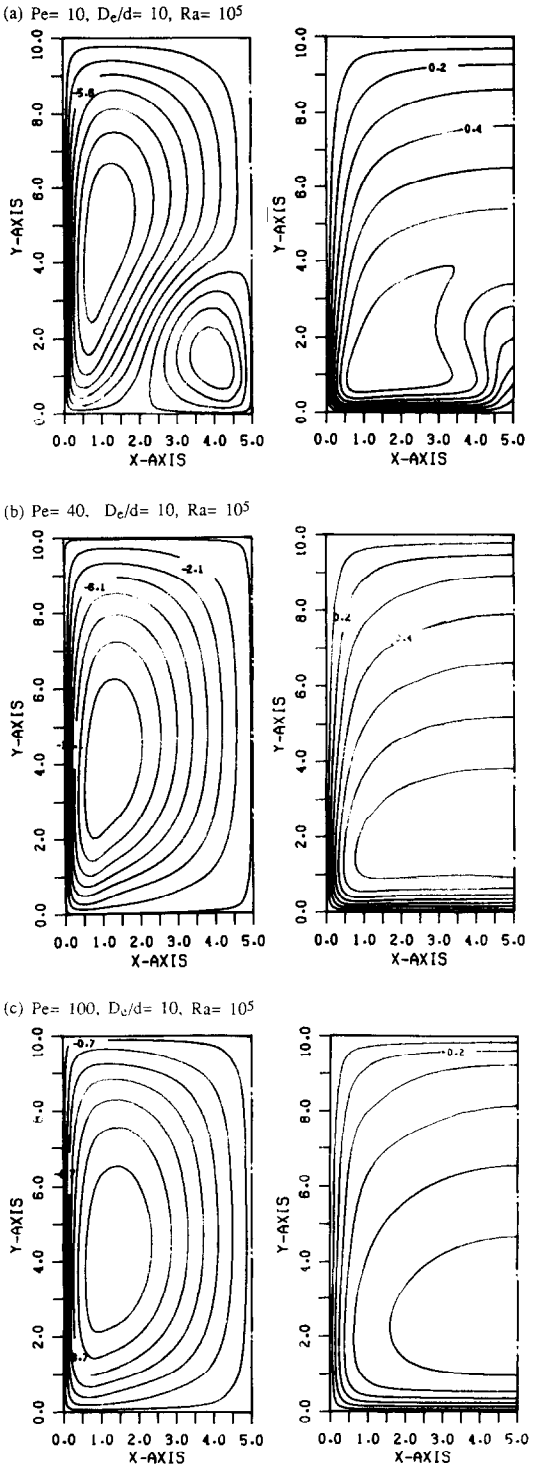

FIG. 3. Isotherm and streamline for $Ra = 10^5$, $Pe = 10$, 40 and 100, and $D_e/d = 10$.

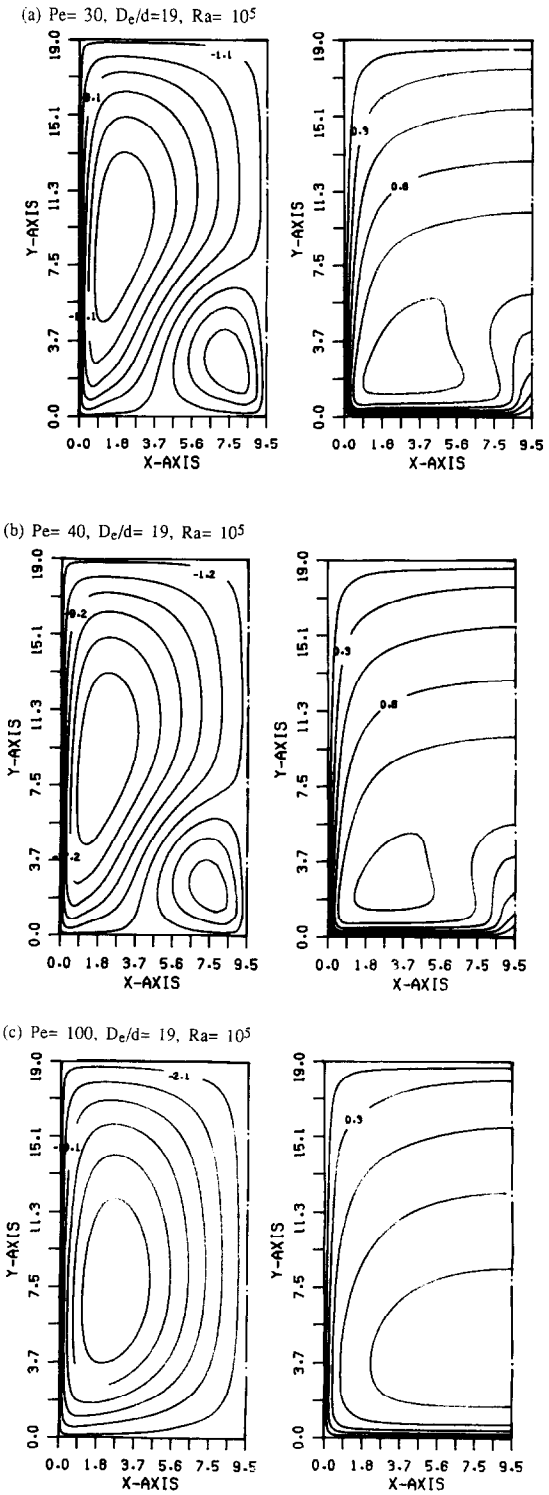

FIG. 4. Isotherm and streamline for $Ra = 10^5$, $Pe = 30$, 40 and 100, and $D_e/d = 19$.

but it changes significantly the patterns of isotherm and streamline when the flow rate becomes high. It is seen in Figs. 3(c) and 4(c) for $Pe = 100$ that the second pair of counter-rotating eddies in the central region near the bottom wall disappear. This result makes sense physically: a relatively uniform temperature distribution is caused by the violent mixing of fluid within the pores in the cases of higher flow rate due to the effect of thermal dispersion, and therefore the magnitude of the adverse temperature gradient decreases

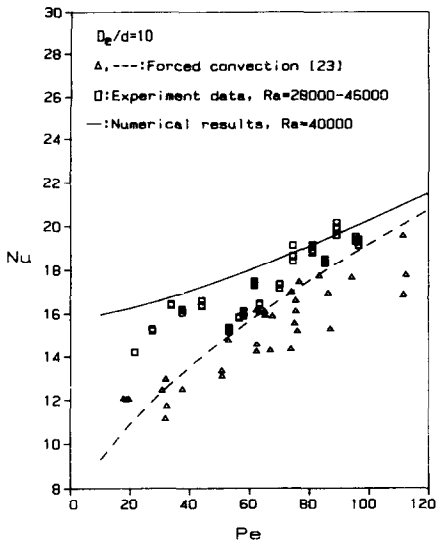

FIG. 5. Theoretical prediction and experimental data of Nusselt number versus Peclet number at certain Rayleigh numbers for $D_e/d = 10$.

and the second pair of counter-rotating eddies is suppressed. It is also seen from Figs. 3(b) and 4(b) for $Ra = 10^5$ and $Pe = 40$ that there is only one pair of eddies in the case of $D_e/d = 10$, but the second pair of eddies appears in the case of $D_e/d = 19$ due to its stronger buoyancy effect.

Comparisons of theoretical predictions of Nusselt number in the fully developed region and experimental measurements of Nusselt number are shown in Figs. 5 and 6 for $D_e/d = 10$ and 19, respectively. It is seen in Fig. 5 for the cases of $D_e/d = 10$ that the theoretical predictions of Nusselt number for $Ra = 4 \times 10^4$ are in agreement with the experimental data for $Ra = 2.8 \times 10^4$–4.6×10^4. By a further comparison with the results of forced convection ($Ra = 0$) [23], it is also seen that the increase of Nusselt number due to the buoyancy effect is higher when the Peclet number is lower. It is seen in Fig. 6 for $D_e/d = 19$ that the theoretical predictions of Nusselt number for $Ra = 2.6 \times 10^4$ are higher than the experimental data for $Ra = 2.6 \times 10^4$–2.9×10^4. This is caused partly by the theoretical overestimation of the thermal dispersion effect, especially in the cases of high Peclet number in the channel of $D_e/d = 19$, because the agreement between the theoretical and experimental results for forced convection is also worse when the Peclet number is high. It is also believed to be caused partly by the entrance effect existing in the experiments because the axial length of the heated section is comparatively too short. In view of the local Nusselt number behavior in the problem of mixed convection in the thermal entrance region of a horizontal square channel without packed spheres [24], it was shown that, except in the region very near the entrance, the entrance effect makes the values of local Nusselt numbers smaller in the thermally developing region than in the fully developed region.

Figures 7 and 8 show the effect of Rayleigh number on the Nusselt number with the Peclet number as a parameter for the cases of $D_e/d = 10$ and 19, respectively. The variation of Nusselt number is found to depend both on the Rayleigh number and Peclet number. This phenomenon is quite different from that in the fluid flow through a channel without packed spheres. For a certain fluid with fixed Prandtl number flowing through a channel without porous media,

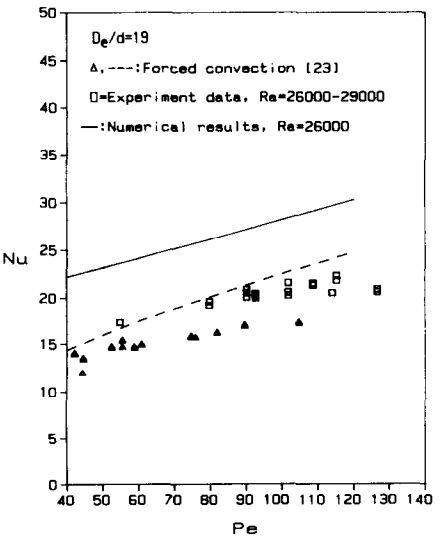

FIG. 6. Theoretical prediction and experimental data of Nusselt number versus Peclet number at certain Rayleigh numbers for $D_e/d = 19$.

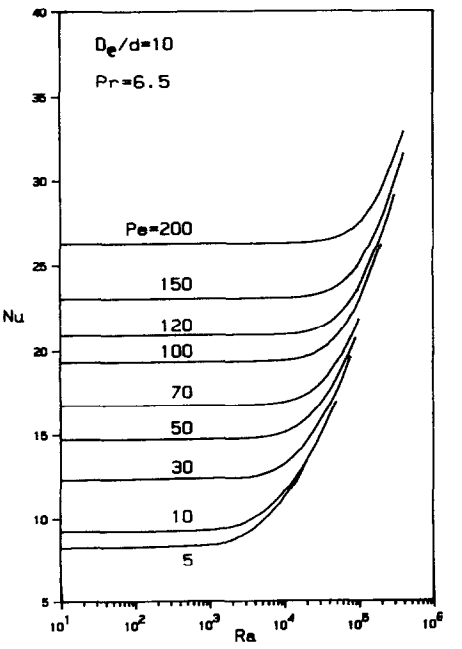

FIG. 7. Nusselt number versus Rayleigh number with Peclet number as a parameter for $D_e/d = 10$.

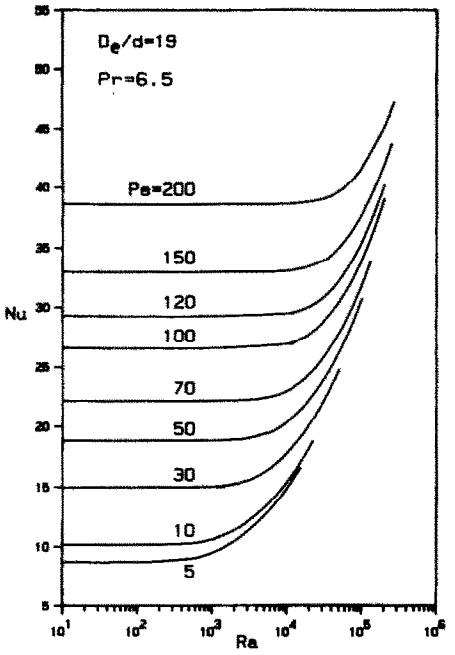

FIG. 8. Nusselt number versus Rayleigh number with Peclet number as a parameter for $D_e/d = 19$.

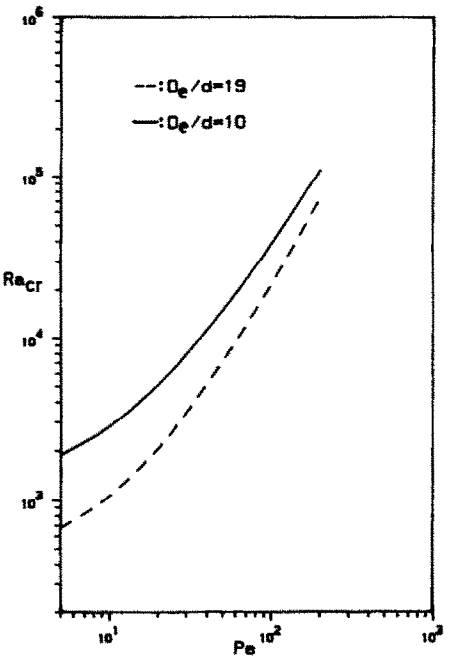

FIG. 9. The critical Rayleigh number for the onset of buoyancy effect based on 5% deviation of Nu from that for forced convection.

the Rayleigh number alone governs the flow and heat transfer characteristics. However, in the present study it is shown that the Nusselt number increases with the increase of Peclet number even for a fixed Rayleigh number; that is, the Rayleigh number and Peclet number govern the flow and heat transfer simultaneously.

Another result is found in Figs. 7 and 8: the value of the Rayleigh number for the onset of the buoyancy effect is delayed as the Peclet number increases. It is interesting to find the relation between the values of Peclet number and critical Rayleigh number, Ra_{cr}, above which the buoyancy effect can no longer be neglected. Based on the criterion of 5% deviation of Nusselt number from that for pure forced convection, the critical Rayleigh number for the onset of the buoyancy effect is found to increase almost exponentially with the increase of Peclet number, as shown in Fig. 9 for both the cases of $D_e/d = 10$ and 19. It is seen that the curve of $D_e/d = 19$ falls below that of $D_e/d = 10$ due to the stronger buoyancy effect in the case of $D_e/d = 19$ even for a fixed Rayleigh number. Therefore for a fixed Peclet number, the onset of the buoyancy effect will occur at lower Rayleigh number in the case of $D_e/d = 19$. The dependence of the critical Rayleigh number for the onset of the buoyancy effect on both the Peclet number and the diameter ratio of channel to sphere is a special phenomenon in porous media, and does not exist in the flow through a channel without packed spheres.

6. CONCLUDING REMARKS

(1) A theoretical model is developed under the consideration of the non-Darcian effects of boundary, inertia, channeling and thermal dispersion to study combined free and forced convection in horizontal square packed-sphere channels. The theoretical prediction of Nusselt number is in good agreement with the experimental data for the $4.75 \times 4.75 \times 85$ cm ($D_e/d = 10$) channel, but the predictions of Nusselt number are higher than the experimental data for the $9.5 \times 9.5 \times 60$ cm ($D_e/d = 19$) channel. This is caused partly by the theoretical overestimation of the thermal dispersion effect, especially in the cases of high Peclet number, and partly by the entrance effect existing in the experiments because the axial length of the heated section is comparatively too short.

(2) From theoretical results, it is found that there exists a higher secondary flow velocity, especially in the region near the vertical wall due to the effects of buoyancy and channeling.

(3) Both the secondary flow pattern and the heat transfer rate are significantly affected by the buoyancy effect when the Peclet number is low. There exists two pairs of counter-rotating eddies for the cases of $Ra = 10^5$, $Pe = 10$ with $D_e/d = 10$, and $Pe = 30$ with $D_e/d = 19$.

(4) The effect of thermal dispersion is to smooth out the temperature distribution, therefore even under a fixed Rayleigh number, the buoyancy effect will be suppressed by the thermal dispersion effect when the Peclet number increases. There is only one pair of eddies for the case of $Ra = 10^5$, $Pe = 100$, and $D_e/d = 10$ and 19. Thus the values of fully developed Nusselt number depend on the values of the Rayleigh number, the Peclet number and the diameter ratio of channel to sphere (D_e/d). The critical Rayleigh num-

ber for the onset of the buoyancy effect increases almost exponentially with the increase of the Peclet number.

Acknowledgement—Financial support for this research provided by the National Science Council of the Republic of China through Grant NSC 79-0401-E008-16 is greatly appreciated.

REFERENCES

1. R. A. Wooding, Convection in saturated porous medium at large Rayleigh number and Peclet number, *J. Fluid Mech.* **15,** 527–544 (1963).
2. M. Prats, The effect of horizontal fluid flow on the thermally induced convection currents in porous medium, *J. Geophys. Res.* **71,** 4835–4837 (1966).
3. F. M. Sutton, Onset of convection in a porous channel with net through flow, *Physics Fluids* **13,** 1931–1934 (1970).
4. G. M. Homsy and A. E. Sherwood, Convective instabilities in porous media with through flow, *A.I.Ch.E. Jl* **22,** 168–174 (1976).
5. M. A. Combarnous and P. Bia, Combined free and forced convection in porous medium, *Soc. Petrol. Engrs J.* **11,** 399–405 (1976).
6. P. Cheng, Combined free and forced boundary layer flows about inclined surface in saturated porous media, *Int. J. Heat Mass Transfer* **20,** 806–814 (1977).
7. P. Cheng, Similarity solutions for mixed convection from horizontal impermeable surface in saturated porous media, *Int. J. Heat Mass Transfer* **20,** 893–898 (1977).
8. W. J. Minkowycz, P. Cheng and R. N. Hirschberg, Non-similar boundary layer analysis of mixed convection about a horizontal heated surface in a fluid-saturated porous medium, *Int. Commun. Heat Mass Transfer* **11,** 127–141 (1984).
9. M. Haajizadeh and C. L. Tien, Combined nature and forced convection in a horizontal porous channel, *Int. J. Heat Mass Transfer* **27,** 799–813 (1984).
10. Y. Joshi and B. Gebhart, Mixed convection in porous media adjacent to a vertical uniform heat flux surface, *Int. J. Heat Mass Transfer* **28,** 1783–1786 (1988).
11. R. H. Oosthuizen, Mixed convection heat transfer from a heated horizontal plate in a porous medium near an impermeable surface, *ASME J. Heat Transfer* **110,** 390–394 (1988).
12. V. Prasad, F. C. Lai and F. A. Kulacki, Mixed convection in horizontal porous layers heated from below, *ASME J. Heat Transfer* **100,** 395–402 (1988).
13. B. C. Chandrasekhara and P. M. S. Namboodiri, Influence of variable permeability on combined free and forced convection about inclined surface in porous media, *Int. J. Heat Mass Transfer* **28,** 199–206 (1985).
14. F. C. Lai and F. A. Kulacki, Non-Darcy convection from horizontal impermeable surface in saturated porous media, *Int. J. Heat Mass Transfer* **30,** 2189–2192 (1987).
15. C. Beckerman and R. Viskanta, Forced convection boundary layer flow and heat transfer along a flat plate embedded in a porous medium, *Int. J. Heat Mass Transfer* **30,** 1547–1551 (1987).
16. P. Cheng and C. T. Zhu, Effect of radial thermal dispersion on fully-developed forced convection in cylindrical packed tubes, *Int. J. Heat Mass Transfer* **30,** 2373–2383 (1987).
17. K. J. Renken and D. Poulikakos, Experiment and analysis of forced convection heat transport in a packed bed of spheres, *Int. J. Heat Mass Transfer* **31,** 1399–1408 (1988).
18. M. L. Hunt and C. L. Tien, Non-Darcian convection in cylindrical packed beds, *ASME J. Heat Transfer* **110,** 378–384 (1988).
19. K. Vafai and C. L. Tien, Boundary and inertia effects on flow and heat transfer in porous medium, *Int. J. Heat Mass Transfer* **24,** 195–203 (1981).
20. R. F. Benenati and C. B. Brosilow, Void fraction distribution in packed beds, *A.I.Ch.E. Jl* **8,** 359–361 (1962).
21. S. Ergun, Fluid flow through packed columns, *Chem. Engng Prog.* **48,** 89–94 (1952).
22. S. M. Kuo and C. L. Tien, Transverse dispersion in packed-sphere beds, *ASME Proc. 1988 Natn. Heat Transfer Conf.*, Houston, pp. 629–634 (1988).
23. F. C. Chou, W. Y. Lien and S. H. Lin, Analysis and experiment of non-Darcian convection in horizontal square packed-sphere channels—I. Forced convection, *Int. J. Heat Mass Transfer* **35,** 195–205 (1992).
24. F. C. Chou and G. J. Hwang, Vorticity–velocity method for the Graetz problem with the effect of natural convection—application to mixed laminar convection in horizontal rectangular channel with uniform wall heat flux, *ASME J. Heat Transfer* **109,** 704–710 (1987).

ANALYSE ET EXPERIENCE DE CONVECTION NON DARCIENNE DANS DES CANAUX CARRES HORIZONTAUX A LIT FIXE—II. CONVECTION MIXTE

Résumé—On présente une analyse et une expérience de convection mixte non darcienne établie dans des canaux horizontaux avec lit de sphères. On considère les effects de non glissement aux frontières, d'inertie, de circuits préférentiels et de dispersion thermique. Les résultats théoriques sont trouvés en accord avec les résultats expérimentaux pour le canal avec $D_c/d = 10$, mais les prédictions du nombre de Nusselt sont supérieures aux données expérimentales à cause de la surestimation théorique de l'effet de dispersion thermique, et de l'effet d'entrée existant dans les expériences pour $D_c/d = 19$. L'analyse montre que l'effet de flottement affecte sensiblement la structure de l'écoulement secondaire et aussi le flux thermique quand le nombre de Peclet est faible. Mais pour un nombre de Rayleigh fixé, l'effet du flottement peut être supprimé lorsque le nombre de Peclet augmente. Les valeurs du nombre de Nusselt dans la région établie dépendent du nombre de Rayleigh, du nombre de Peclet et du rapport des diamètres du canal et de la sphère (D_c/d).

ANALYTISCHE UND EXPERIMENTELLE UNTERSUCHUNG DER KONVEKTION AUSSERHALB DES DARCY'SCHEN BEREICHS IN EINEM WAAGERECHT DURCHSTRÖMTEN, QUADRATISCHEN FESTBETT AUS KUGELN—II. MISCHKONVEKTION

Zusammenfassung—In der vorliegenden Arbeit wird über analytische und experimentelle Untersuchungen der vollständig entwickelten Mischkonvektion außerhalb des Darcy'schen Bereichs in einem waagerecht durchströmten Festbett aus Kugeln berichtet. Folgende nicht-Darcy'schen Effekte werden berücksichtigt: Haftbedingungen an der Grenzfläche, Trägheit der Strömung, Kanalbildung und thermische Dispersion. Die theoretischen Ergebnisse stimmen mit den Versuchsergebnissen für den Kanal $D_c/d = 10$ überein. Die berechneten Nusselt-Zahlen sind jedoch größer als die entsprechenden Versuchsergebnisse. Dies wird teilweise darauf zurückgeführt, daß die theoretische Berechnung die thermische Dispersion überbewertet, teilweise auf Eintrittseffekte bei Versuchen mit $D_c/d = 19$. Die analytische Untersuchung zeigt, daß der Auftriebseffekt die Struktur der Sekundärströmung und den Wärmeübergang wesentlich beeinflußt-dies gilt für kleine Peclet-Zahlen. Der Auftriebseffekt wird hingegen unterdrückt, wenn die Peclet-Zahl zunimmt, sogar bei festgehaltener Rayleigh-Zahl. Die Nusselt-Zahl im vollständig entwickelten Gebiet hängt von der Rayleigh-Zahl, der Peclet-Zahl und dem Durchmesserverhältnis von Kanal und Kugel (D_c/d) ab.

АНАЛИТИЧЕСКОЕ ЭКСПЕРИМЕНТАЛЬНОЕ ИССЛЕДОВАНИЕ КОНВЕКЦИИ В ГОРИЗОНТАЛЬНЫХ КАНАЛАХ КВАДРАТНОГО СЕЧЕНИЯ С УПАКОВКАМИ СФЕР

Аннотация—Аналитически и экспериментально исследуется полностью развитая смешанная конвекция в горизонтальных каналах с упаковками сфер. Рассматриваются эффекты, вызывающие отклонение от закона Дарси и обусловленные условиями прилипания на границах, иенрцией течения, тепловой дисперсией. Найдено, что теоретические результаты согласуются с экспериментальными данными, полученными для канала с $D_c/d = 10$, но расчетные значения числа Нуссельта превымают результаты экспериментов частично из-за эффекта входа, присутствующего в экспериментах для $D_c/d = 19$. Анализ показывает, что подъемная сила оказывает существенное влияние на структуру вторичного течения и скорость теплопереноса при низком числе Пекле, но оно может при постоянном числе Рэлея уменьшаться с ростом числа Пекле. Значения числа Нуссельта в полностью развитой области зависят от значений чисел Рэлея и Пекле, а также от отношения диаметров канала и сферы D_c/d.